PAN POLSKA AKADEMIA NAUK

METROLOGY AND MEASUREMENT SYSTEMS

Index 330930, ISSN 0860-8229

www.metrology.pg.gda.pl

M&MS

AN IMPROVED RESONANT THERMAL CONVERTER BASED ON MICRO-BRIDGE RESONATOR

Lizhen Dong, Jianqiang Han, Peng Zhang, Zhengqian Zhao, Bing Cheng, Dong Han

China Jiliang University, The College of Mechanical & Electrical Engineering, Hangzhou, 310018, China
(*18767105003@163.com*, ✉ *hjqsmx@sina.com*, +86 188 6876 5369, *1051009451@qq.com*, *994556402@qq.com*, *1012046860@qq.com*, *734233043@qq.com*)

Abstract

This paper presents the design, fabrication and testing of an improved thin-film thermal converter based on an electro-thermally excited and piezo-resistively detected micro-bridge resonator. The resonant thermal converter comprises a bifilar heater and an opposing micro-bridge resonator. When the micro-bridge resonator absorbs the radiant heat from the heater, its axial strain changes, then its resonant frequency follows. Therefore the alternating voltage or current can be transferred to the equivalent DC quantity. A non-contact temperature sensing mechanism eliminates heat loss from thermopiles and reduces coupling capacitance between the temperature sensor and the heater compared with traditional thin-film thermal converters based on thermopiles. In addition, the quasi-digital output of the resonant thin-film thermal converter eliminates such problems as intensity fluctuations associated with analogue signals output by traditional thin-film thermal converters. Using the fast-reversed DC (FRDC) method, the thermoelectric transfer difference, which determines the frequency-independent part of the ac-dc transfer difference, is evaluated to be as low as $1.1 \cdot 10^{-6}$. It indicates that the non-contact temperature sensing mechanism is a feasible method to develop a high-performance thermal converter.

Keywords: thermoelectric transfer difference, micro-bridge resonator, thermal converter, bifilar heater.

1. Introduction

The most accurate method for transferring alternating voltage or current to the equivalent DC quantity is using *thermal converters* (TCs) [1–3]. They can be divided into four types: *single-junction thermal converters* (SJTCs) [4], 3D *multi-junction thermal converters* (3D MJTCs) [5], *thin-film (or planar) thermal converters* (FMJTCs) [6–10] and semiconductor *root mean square* (RMS) sensors [11]. Thin-film thermal converters are today's most accurate standard for precise measuring the RMS of AC quantities in a frequency range of 10 Hz–1 MHz. A typical thin-film thermal converter based on thermopiles comprises a heater and a thermopile [12]. The heater and hot junctions of the thermopile are placed on the top surface of a stress-compensated sandwich membrane; cold junctions of the thermopile are placed on the silicon substrate acting as a heat sink [6–10]. The ac and dc voltage (or current) are applied sequentially to the heater and heat it. The temperature sensor senses the temperature field. As the output signal

Article history: received on May 30, 2018; accepted on Aug. 14, 2018; available online on Dec. 31, 2018, DOI: 10.24425/mms.2018.124882.

of the temperature sensor is identical, the dc voltage (or current) is the RMS of the ac voltage (or current). The nearly periodic structure of the thermal element results in a constant temperature along the bifilar heater, reducing the ac-dc transfer difference caused by the Thomson effect.

The coupling capacitance between the heater and the hot junctions of thermopiles and the heat conduction of the heater from the thermopiles to the substrate are the main sources of thermoelectric transfer difference. A feasible way to solve these two problems is to utilize non-contact temperature sensing [13]. The non-contact temperature sensing method can minimize the detrimental effects caused by thermal and electrical shunt paths in conventional thermal elements [14]. The ac-dc transfer difference caused by coupling capacitance can be remarkably reduced. It the potential for greater accuracy over a wide frequency range, faster response time, and improved dynamic range over conventional planar thermal elements. However, the reported non-contact film thermal converters are only simple combination of a heater and a commercial temperature sensing element. The ac-dc voltage transfer differences of the non-contact thermal converters are as high as 20×10^{-6} to 50×10^{-6} for a thermal converter with infrared-transmission fibre coupling [15] and 140×10^{-6} for a thermal converter with radiometric sensing at 1 MHz [16]. However, these methods of non-contact temperature sensing techniques have not received much attention to date.

Minimizing the thermoelectric transfer difference of a thermal converter must reduce the capacitive coupling between the heater and the hot junctions of thermopiles and eliminate the heat conduction of the heater from the temperature sensing element to the substrate. In the previous work, our study team proposed a prototypical resonant thermal converter consisting of a heater and a micro-bridge resonator placed side by side on one chip [17]. Since the micro-bridge resonator is not directly opposite to the heater, only a small part of the heat of the heater is conducted to the bridge resonator. This defect causes a lower temperature sensitivity of the bridge resonator and a larger thermoelectric transfer difference of $2.8 \times 10^{-6} \sim 9.1 \times 10^{-6}$ at the frequency range of $10^2 \sim 10^4$ Hz exhibited by the thermal converter. In this paper, an improved non-contact thin film thermal converter based on a micro-bridge resonator and an opposite heater is proposed to measure the thermoelectric transfer difference.

2. Structures and process

2.1. Structure of improved film thermal converter

The improved film thermal converter comprises a micro-bridge resonator and an opposing bifilar heater. The length and width of the micro-bridge are 1000 μm and 100 μm, respectively. The length and width of the bifilar heater are 950 μm and 100 μm, respectively. The bridge resonator and the bifilar heater are fabricated on different silicon wafers and assembled together by the eutectic bonding process. The $Ni_{24.9}Cr_{72.5}Si_{2.6}$ heater is placed on SiO_2/Si_3N_4 bilayer films and covered with a 0.42 μm Si_xN_y film. The bifilar structure of the heater can effectively reduce the thermoelectric transfer difference caused by the Thomson effect [18]. The micro-bridge consists of a 0.6 μm silicon dioxide film, a 0.25 μm Si_3N_4 film deposited by *low pressure chemical vapor deposition* (LPCVD) and a 0.42 μm Si_xN_y film deposited by *plasma-enhanced chemical vapor deposition* (PECVD). The configuration of developed resonant thin-film thermal converter is shown in Fig. 1.

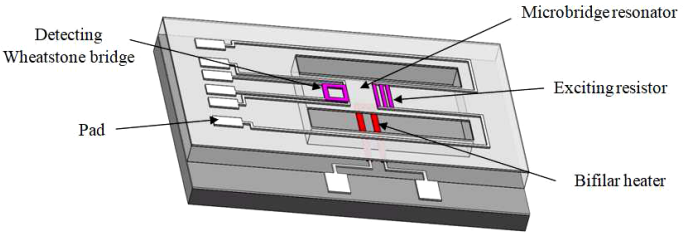

Fig. 1. The configuration of developed resonant thin-film thermal converter.

2.2. Fabrication process of heater

1. The fabrication process of the heater starts from (100) oriented, n-type silicon wafers. The wafers are cleaned and thermally oxidized in the first step. The thickness of silicon dioxide is 0.6 μm. Then, a 0.25 μm Si_3N_4 film is deposited by low pressure chemical vapor deposition (LPCVD) at 1053.15 K, as shown in Fig. 2 a.The compressive stress of the SiO_2 film is compensated by the tensile stress of the Si_3N_4 film.
2. An 89 nm thick $Ni_{24.9}Cr_{72.5}Si_{2.6}$ film is deposited by the *radio frequency* (RF) magnetron sputtering technique on the front surface. Bifilar heaters are patterned and etched in ammonium ceric nitrate solution. The Ti/Au metallization system is used as wires and bonding material placed on the ambitus of chip. The wafers are annealed at 400 °C in N_2 atmosphere for 30 minutes to strengthen adhesion between the Ti/Au film and the Si_3N_4 film, as shown in Fig. 2b.
3. A 0.42 μm Si_xN_y film used as a passivated layer of the heater is deposited by the *plasma-enhanced chemical vapor deposition* (PECVD) process on the front side of wafers. The Si_xN_y film on the pads is patterned and etched by *inductively coupled plasma* (ICP) dry etching, as shown in Fig. 2c.
4. Openings below the heater are patterned and etched. Using the silicon dioxide and silicon nitride films as mask, the silicon beneath the heater is etched away in 40% KOH solution to 30 μm and then etched by ICP dry etching, as shown in Fig. 2d.

2.3. Fabrication process of micro-bridge resonators

1. The fabrication process the micro-bridge resonator starts also from (100) oriented, n-type silicon wafers. A 0.6 μm silicon dioxide film and a 0.25 μm LPCVD Si_3N_4 film are deposited sequentially on both sides of the wafer, as shown in Fig. 2e.
2. A 0.65 μm polysilicon film is deposited by *low pressure chemical vapour deposition* (LPCVD) at 893.15 K. Boron ions are implanted in the polysilicon film. The implantation energy and dose are 80 KeV and 1.7×10^{15} cm^{-2}, respectively. The implanted boron atoms are activated in nitrogen at 1223.15 K. The doped polysilicon film is patterned and dry etched to form polysilicon resistors at the middle of resonant beams for driving the resonant beams and – at the clamped end of resonant beams – to detect the vibration. A 0.8 μm aluminium film is deposited on the front side of the wafers by DC sputtering and patterned for the electrical connection. The pads connected to the heater are placed on the silicon frame, insulated by SiO_2 and Si_3N_4 films. Peltier heat will, therefore, be short-circuited. Then, the wafers are annealed at 450°C in N_2 atmosphere for 30 minutes to form a good ohmic contact between the Al and doped polysilicon films, as shown in Fig. 2f.

3. A 0.42 μm Si_xN_y film used as a passivated layer of polysilicon resistors is deposited by the *plasma-enhanced chemical vapour deposition* (PECVD) process on the front side of wafers. The Si_xN_y film on the pads is patterned and etched by ICP dry etching, as shown in Fig. 2g.
4. The bridge along the <110>direction is patterned on the front side of wafer. The Si_xN_y film, Si_3N_4 film and SiO_2 film in the groove are etched by ICP dry etching. A window below the bridge is patterned on the backside of the wafer. Anisotropic wet etching through the window is carried out in KOH solution to thin the wafer to 30 μm while protecting the front side in a mechanical chuck. A 0.47 μm amorphous silicon film is deposited on the backside of wafers for eutectic bonding with an Au film on the micro-bridge resonator chips. Then, the beams are released by the *reactive ion etching* (RIE) process, as shown in Fig. 2h.

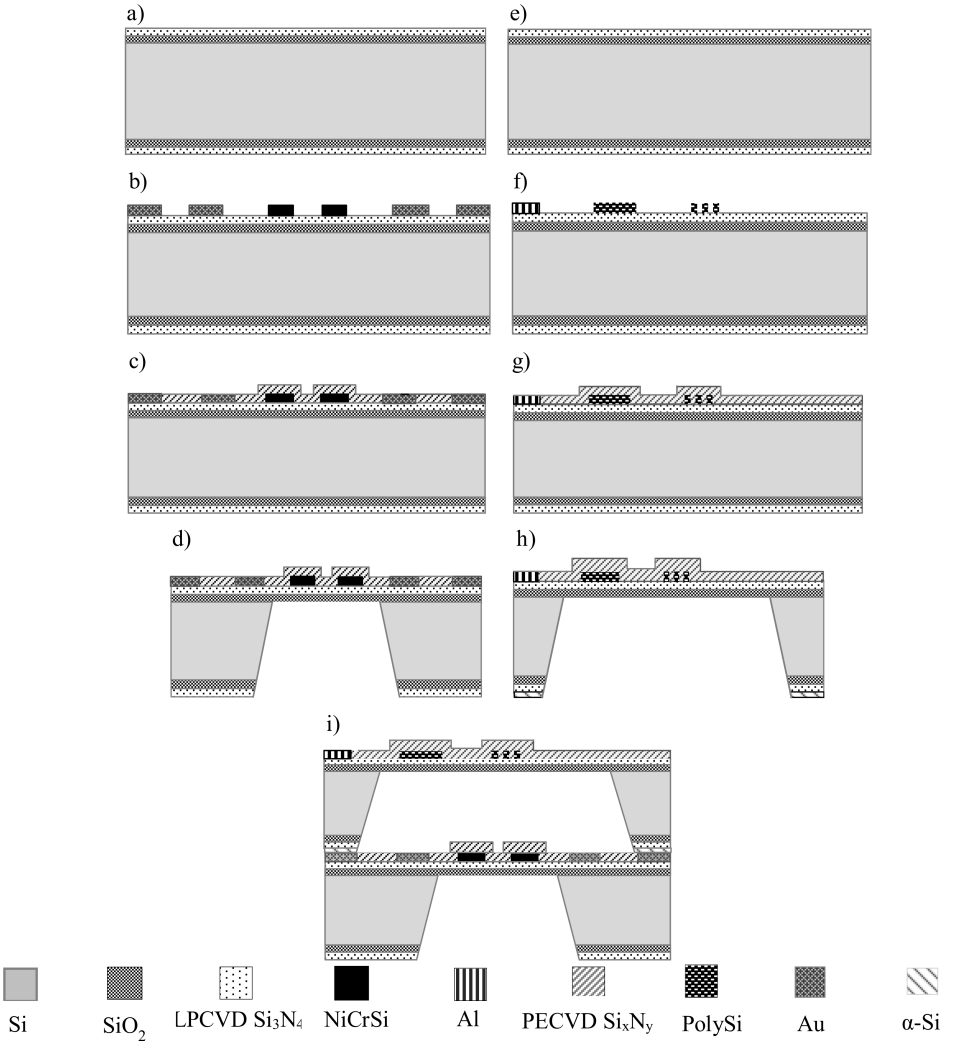

Fig. 2. The fabrication process of the thermal converter based on a micro-bridge resonator. a)–d) the fabrication process of the heater; e)–h) the fabrication process of the micro-bridge resonator; i) the bonded resonant thin-film thermal converter.

2.4. Gold-amorphous silicon bonding process

The amorphous silicon at the backside of the micro-bridge resonator chip and the Au film on the front side of the heater chip are bonded together with the eutectic bonding process. An Ar plasma pre-treatment is carried out to remove contaminants and 1:50 HF solution is used to remove any native oxide at the surface of amorphous silicon before the bonding process. The Au-amorphous silicon eutectic bonding process is performed in a vacuum chamber with a vacuum degree of 10^{-3} Pa. The bonding temperature and pressure are 430° and 0.75 MPa, respectively. A cross-section view of the bonded resonant thin-film thermal converter is shown in Fig. 2i. *Scanning Electron Microscope* (SEM) images of the developed resonant thin-film thermal converter are shown in Fig. 3.

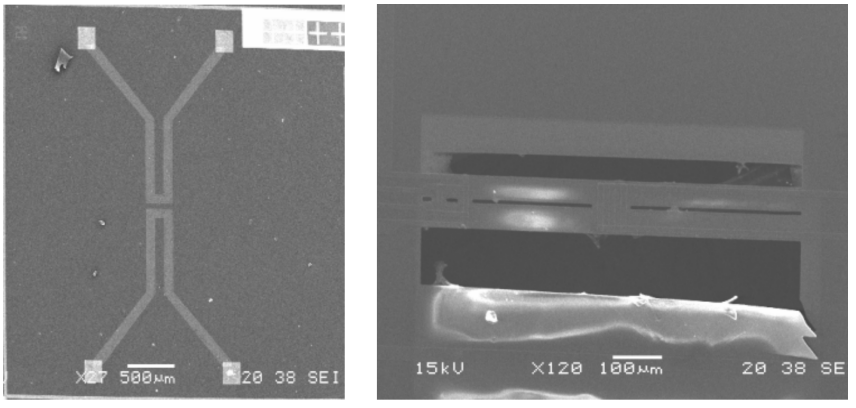

Fig. 3. SEM images of the fabricated heater (left) and micro-bridge resonator (right).

3. Detection mechanisms

The first-order flexural resonance frequency of a micro-bridge resonator is [19]:

$$f_1(\varepsilon) = 1.029\frac{h}{L^2}\sqrt{\frac{E}{\rho(1-\nu^2)}}\sqrt{1+0.2949\varepsilon(1-\nu^2)\left(\frac{L}{h}\right)^2} \tag{1}$$

where: L, h and ε are the length, thickness and axial strain of the micro-bridge and ν, E and ρ are Poisson's ratio, equivalent Young's modulus and density of the material.

The sensitivity of the micro-bridge resonator to the absorbed heat power (P) can be calculated as [20]:

$$\frac{df_1(\varepsilon)}{f_1 dP} = \frac{0.2949(1-\nu^2)\left(\frac{L}{h}\right)^2}{2\left[1+0.2949\varepsilon(1-\nu^2)\left(\frac{L}{h}\right)^2\right]}\frac{d\varepsilon}{dP}. \tag{2}$$

Assuming that the length between two clamped ends remains constant after the bridge absorbs the heat radiation of heater, the axial strain of the micro-bridge can be expressed as:

$$\varepsilon = \varepsilon_0(\alpha - \alpha_{si})\Delta T_{av}(P), \tag{3}$$

where ε_0 is the original axial strain of the micro-bridge resonator arose in the fabrication process and is the average thermal expansion coefficient of materials composing the micro-bridge.

$$\overline{\alpha} = \frac{\sum \alpha_i E_i h_i}{\sum E_i h_i} . \tag{4}$$

$\Delta T_{av}(P)$ is the average temperature elevation of the micro-bridge due to the heat radiation from the $Ni_{24.9}Cr_{72.5}Si_{2.6}$ resistor. Fig. 4 shows the original temperature distribution (ΔT_1) of the micro-bridge under 1 mW alternating excitation power at the excitation resistor and 9 mW Joule heat generated at the Wheatstone bridge. The temperature of the micro-bridge rises to ΔT_2 if a 10 mW heating power is applied to the $Ni_{24.9}Cr_{72.5}Si_{2.6}$ heater. The temperature elevation ($\Delta T_2 - \Delta T_1$) reduces the axial tensile strain or increases the compressive strain of the micro-bridge resonator, thereby changing its resonant frequency.

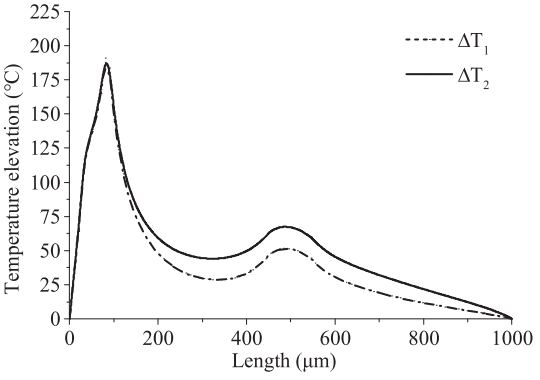

Fig. 4. The temperature distribution of the micro-bridge along the length direction.

4. Thermoelectric transfer difference

4.1. Testing system based on fast reversed DC-source

The thermoelectric transfer difference determines the frequency-independent part of the ac-dc transfer difference. It has been widely measured with a FRDC source [21–24]. The *fast reversed DC-experiment* (FRDC) provides an independent and simple means of evaluating thermoelectric effects in any type of thermal converter constructions, but with a sub-ppm level of uncertainty [24]. This method is based on the fact that the modification of the temperature distribution along the heater due to the Thomson and Peltier effects depends on the direction of the dc current. If the current reverses, the modification will be built-up in the other direction, which spends some time due to the thermal time constant of the converter. With increasing the reversing frequency, the change of temperature caused by thermoelectric effects is reduced to zero.

The test system based on a computer-controlled FRDC source to measure thermoelectric transfer difference of the resonant thermal converter consists of a signal generation module, a thin film thermal converter, a constant temperature platform and a signal processing and data acquisition module [17]. A block diagram of the system is shown in Fig. 5. The signal generation module includes an FRDC source and a *field-programmable gate array* (FPGA). The FRDC source consists of two identical reference voltage sources A and B that are alternately opened

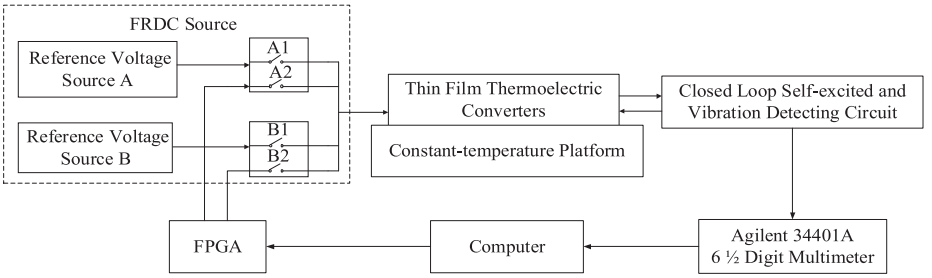

Fig. 5. The computer-controlled testing system based on a fast reversed DC-source.

and closed to reduce the power loss caused by the voltage polarity reversal. The FPGA controls the closing and opening of the switch array to generate the FRDC and CPDC (Chopped DC) signals alternately applied to the heater. The thin-film thermal converter is placed on the constant temperature platform to keep its temperature constant, thereby reducing the impact of ambient temperature on the thermoelectric transfer difference. The thermostatic platform based on a *thermoelectric cooler* (TEC) thermostat ADN8830 chip is used to maintain the temperature of the thermoelectric converter varying within $\pm 0.01^{\circ}$. The closed-loop self-excited and oscillating circuit [25] enables the micro-bridge resonator to operate in a self-oscillation state. The Agilent 34401A 6 1/2 digit multi-meter is used to collect the output frequency of the resonant thermal converter and to transfer the frequency to a virtual frequency meter programmed by LabVIEW via RS232 serial communication interface.

4.2. Measuring principle

The FRDC source controlled by FPGA outputs sequentially four different signals [17], named FRDC(1), CPDC(+), CPDC(−) and FRDC(2), as shown in Fig. 6. Each signal is generated by switching between stable dc levels and zero potential. For the FRDC(1) and FRDC(2) signals, the voltage is alternately reversed in the positive and negative polarity. The CPDC(+) and CPDC(−) signals have a constant output level except for brief transitions to zero.

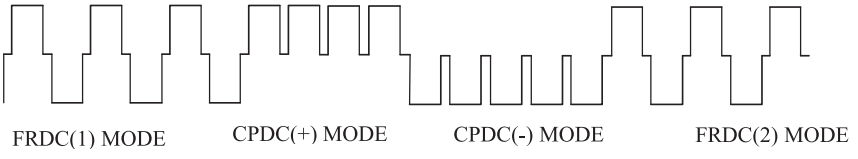

Fig. 6. The output signals of the FRDC source.

In order to measure the thermoelectric transfer difference, the four signals FRDC(1), CPDC(+), CPDC(−) and FRDC(2) are sequentially applied to the heater. The duration and interval of each signal is 2 minutes. The amplitude of the FRDC and CPDC signals applied to the heater is 2.333 V, which corresponds to a heating power of 10.12 mW. The output resonant frequency of the resonant thermal converter for 5 kHz FRDC and CPDC signals applied to the heater is shown in Fig. 7. The resonant frequency of the micro-bridge resonator decreases by 73.6 Hz when the PRDC or CPDC signals are applied to the heating resistor. The relative shift of resonant frequency is 350 ppm/mW, while the relative frequency shifts of the early device

[17] is only 220 ppm/mW. It shows that the novel thermal converter has a higher temperature measurement sensitivity.

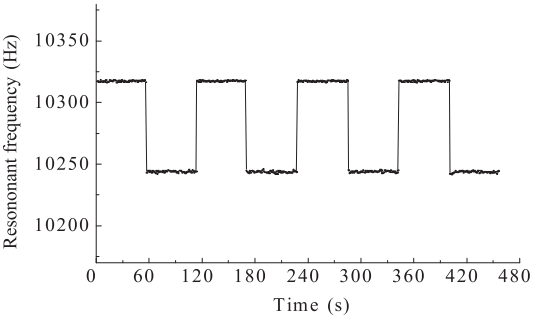

Fig. 7. The output frequency of the resonant thermal converter for 5 kHz FRDC and CPDC signals applied to the heater.

The thermoelectric transfer difference is calculated as:

$$\delta = -\frac{f_{\mathrm{FRDC}} - f_{\mathrm{CPDC}}}{n f_{\mathrm{CPDC}}}, \tag{5}$$

where: f_{FRDC} is the average resonant frequency of the bridge resonator when the FRDC(1) and FRDC(2) signals are applied to the heater, respectively; f_{CPDC} is the average resonant frequency when the CPDC(+) and CPDC(−) signals are applied, respectively and n is a normalized index that indicates the characteristics of the input–output responses of a thermal converter. As shown in Fig. 8, the normalized index can be determined from a curve of the resonance frequency shift (Δf) of the micro-bridge resonator and DC voltages (V) applied to the heater and then fitted in the equation $\Delta f = \mathrm{kV}^n$. The normalized index value is about 1.907, which is larger than that of a traditional the early thermal converter ($n = 1.59$). It shows that the frequency shift of the bridge resonator is larger for the same input voltage, thus the thermal converter presented in this paper has a greater temperature measurement sensitivity, although the distance between the temperature sensor and the heater increased from 70 μm to 375 μm.

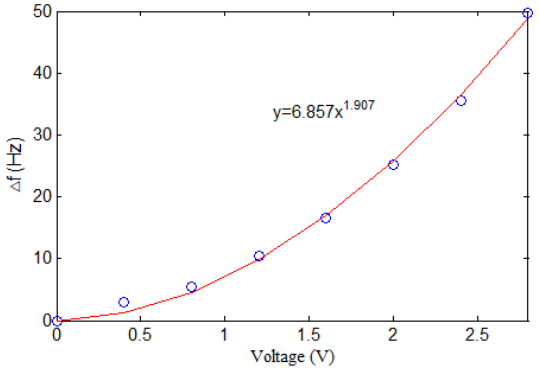

Fig. 8. The resonant frequency shift of the micro-bridge resonator for voltages applied to the heater.

4.3. Measuring results

Thermoelectric transfer differences of the resonant thermal converters at different frequencies are shown in Fig. 9. The thermoelectric transfer difference of this resonant thermal converter is $1.1 \times 10^{-6} \sim 5.4 \times 10^{-6}$ in a frequency range of $10^2 \sim 10^4$ Hz. Compared with that of $2.8 \times 10^{-6} \sim 9.1 \times 10^{-6}$ of the early thermal converter [17], the improved resonant thermal converter reduces the thermoelectric transfer difference mainly because the micro-bridge resonator is opposed to the bifilar heater. This structural improvement causes that the new device has a higher temperature measurement sensitivity.

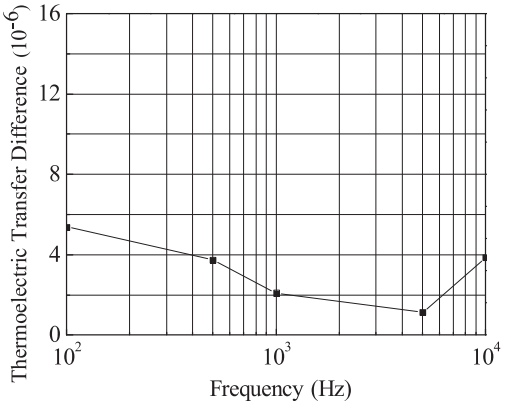

Fig. 9. Thermoelectric transfer differences of the resonant thermal converters at different frequencies.

Figure 10 shows the frequency response of the resonant thermal converter when a 2.333 V step voltage is applied to the heater. It indicates that the time constant of the improved resonant thermal converter is about 460 ms. Compared with the 280 ms of the thermal converter developed in the previous work [17] and 25 ms of traditional thin-film thermal converters based on thermopiles without silicon obelisk [26], the time constant obviously increased because of a greater distance between the micro-bridge resonator and the heater. The improved time constant will reduce the ac–dc transfer difference at low frequencies [26–27].

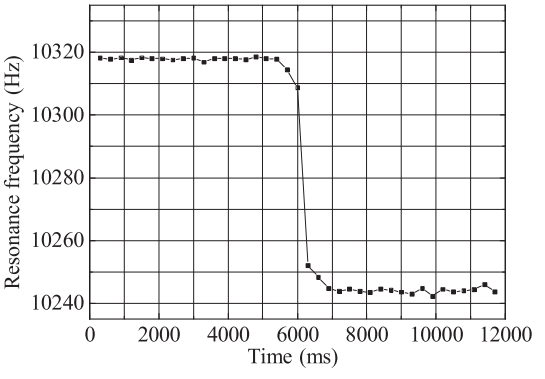

Fig. 10. The frequency response of the resonant thermal converter.

5. Conclusion

This paper presents an improved thin-film thermal converter based on a micro-bridge resonator. Compared with earlier thermal converters, the improved resonant thermal converter comprises a bifilar heater and an opposing micro-bridge resonator. Owing to this structural improvement, the new device exhibits three following advantages: (1) the temperature measurement sensitivity is increased from 220 ppm/mW to 350 ppm/mW. (2) The thermoelectric transfer difference is reduced from $2.8 \times 10^{-6} \sim 9.1 \times 10^{-6}$ to $1.1 \times 10^{-6} \sim 5.4 \times 10^{-6}$ at a frequency range of $10^2 \sim 10^4$ Hz. (3) The greater distance between the micro-bridge resonator and the heater increases the time constant, reduces the ac-dc transfer difference at low frequencies and reduces the coupling capacitance between the heater and the temperature sensor. Further optimization of the device structure is underway and will be reported in the future.

Acknowledgements

The authors would like to acknowledge the financial support from the Natural Science Foundation of China (61376114,51377025).

References

[1] Klonz, M., Weimann, T. (2002). Accurate thin film multijunction thermal converter on a silicon chip (ac-dc standard). *IEEE Transactions on Instrumentation & Measurement*, 38(1), 335–337.

[2] Scarioni, L., Klonz, M., Funck, T., Kessler, E. (2006). New generation of crystal quartz thin-film multijunction thermal converters. *IEEE Transactions on Instrumentation & Measurement*, 55(6), 2281–2285.

[3] Lipe, T.E., Kinard, J.R., Novotny, D.B. (2012). New high-frequency MJTCs of novel design on fused silica substrates. *Precision Electromagnetic Measurements IEEE*, 434–435.

[4] Bubanja, V. (2000). The ac-dc difference of single-junction thermal converters. *Journal of Engineering Mathematics*, 38(1), 33–50.

[5] Kinard, J.R., Huang, D.X., Novotny, D.B. (1994). Multilayer film multijunction thermal converters. *WO*, 1994016464 A1.

[6] Klonz, M., Weimann, T. (1998). Accurate Thin Film Multijunction Thermal Converter on a Silicon Chip. *Precision Electromagnetic Measurements, CPEM 88 Digest. Conference on IEEE*, 215–216.

[7] Scarioni, L., Klonz, M., Kebler, E. (2007). Explanation for the ac–dc voltage transfer differences in thin-film multijunction thermal converters on silicon chips at high frequencies. *IEEE Transactions on Instrumentation & Measurement*, 56(1), 567–570.

[8] Kim, J.S., Lee, H.C., Lee, J.H., Lee, J.H., Park, S.I., Kwon, S.W. (2002). A planar bi-sb multijunction thermal converter with small ac-dc transfer differences. *IEEE Transactions on Instrumentation & Measurement*, 51(1), 115–119.

[9] Fujiki, H., Kasai, N., Sasaki, H., Shoji, A. (2004). High-Performance Thin-Film Multijunction Thermal Converter Developed at AIST. *Precision Electromagnetic Measurements Digest, 2004 Conference on IEEE*, 459–460.

[10] Laiz, H., Klonz, M., Kessler, E., Kampik, M., Lapuh, R. (2003). Low-frequency ac-dc voltage transfer standards with new high-sensitivity and low-power-coefficient thin-film multijunction thermal converters. *IEEE Transactions on Instrumentation & Measurement*, 52(1), 350–354.

[11] Abdulrazzaq, B.I., Ibrahim, O.J., Kawahito, S., Sidek, R.M., Shafie, S., Yunus, N.A., *et al*. (2016). Design of a sub-picosecond jitter with adjustable-range cmos delay-locked loop for high-speed and low-power applications. *Sensors*, 16(10).

[12] Dintner, H., Klonz, M., Lerm, A., Volklein, F., Weimann, T. (2002). Ac-dc-mv-transfer with highly sensitive thin-film multijunction thermal converters. *IEEE Transactions on Instrumentation & Measurement*, 42(1), 612–614.

[13] Katzmann, F.L. (1989). A new isothermal multijunction differential thermal element provides fast settling ac to dc converter. *IEEE Transactions on Instrumentation & Measurement*, 38(1), 346–350.

[14] Katzmann, F.L., Stollery, D.E. (1993). A new optically sensed thermal element for precise ac-dc conversion. *IEEE Transactions on Instrumentation & Measurement*, 42(1), 191–194.

[15] Katzmann, F.L., Klonz, M. (1998). Ac-dc thermal converter with infrared-transmissive fiber coupling. *IEEE Transactions on Instrumentation & Measurement*, 48(1), 415–417.

[16] Katzmann, F.L., Klonz, M. (1995). Fast thin-film isothermal ac-dc converter with radiometric sensing. *IEEE Transactions on Instrumentation & Measurement*, 44(1), 391–394.

[17] Han, J., Huang, R., Zhang, P., Cheng, B., Dong, L., Han, D. (2018). A novel film thermal converter based on an electrothermally excited/piezoresistively detected microbridge resonator. *IEEE Transactions on Instrumentation & Measurement*, 99, 1–9.

[18] Katzmann, F.L., Klonz, M. (1994). A thin-film dual heater ac-dc converter with infrared sensor. *Precision Electromagnetic Measurements. Digest. 1994 Conference on IEEE*, 413–414.

[19] Tilmans, H.A.C., Elwenspoek, M., Fluitman, J.H.J. (1992). Micro resonant force gauges. *Sensors & Actuators A Physical*, 30(1–2), 35–53.

[20] Han, J.Q., Sen-Lin, L.I., Yan, L.I., Wang, X.F., Feng, R.S. (2015). Resonant IR detectors based on microbridge resonators electrothermally excited and piezoresistively detected using polysilicon resistors of negative tTCR. *Journal of Infrared & Millimeter Waves*, 34(1), 134–139.

[21] Klonz, M., Spiegel, T., Zirpel, R., Inglis, B.D., Hammond, G., Sasaki, H. (2002). Measuring thermoelectric effects in thermal converters with a fast reversed dc. *IEEE Transactions on Instrumentation & Measurement*, 44(1), 379–382.

[22] Sasaki, H., Takahashi, K., Klonz, M., Endo, T. (1993). High-precision AC-DC transfer standards at ETL. *IEEE Transactions on Instrumentation & Measurement*, 42(1), 603–607.

[23] Sasaki, H., Takahashi, K., Klonz, M. (1994). Development of a fast-reversed-dc current source. *Precision Electromagnetic Measurements Digest, 1994 Conference on IEEE*, 386–387.

[24] Klonz, M., Spiegel, T., Sasaki, H., Takahashi, K. (1996). Fast reversed dc: basic reference for ac-dc transfer. *Precision Electromagnetic Measurements Digest, 1996 Conference on IEEE*, 501–502.

[25] Han, J.Q., Wang, X.F., Feng, R.S. (2012). Dependence of the Resonance Frequency of Mircobridge Resonators on the Thermal Power and Vacuum. *Advanced Materials Research*, 465, 14–22.

[26] Klonz, M., Laiz, H., Kessler, E. (2001). Development of thin-film multijunction thermal converters at ptb/ipht. *IEEE Transactions on Instrumentation & Measurement*, 50(6), 1490–1498.

[27] Klonz, M., Weimann, T. (1991). Increasing the time constant of a thin film multijunction thermal converter for low frequency application. *IEEE Transactions on Instrumentation & Measurement*, 40(1), 350–351.